In preparation
Preprint typeset using LaTeX style emulateapj v. 01/23/15

NEAR INFRARED SPECTRUM OF A CLASS 0 PROTOSTAR PHOTOSPHERE

Thomas P. Greene, Michael A. Gully-Santiago
NASA Ames Research Center, Space Science and Astrobiology Division, M.S. 245-6; Moffett Field, CA 94035

M. Barsony
SETI
In preparation

ABSTRACT

We measure the stellar photosphere of a Class 0 protostar.

Subject headings: stars: fundamental parameters — stars: individual (S68N) — stars: low-mass – stars: statistics

1. INTRODUCTION

todo: T.P.G introductory text

2. OBSERVATIONS

The observations of S68N were carried out with NIRSPEC on the Keck telescope over 5 epochs from 2003-2014. The `NIRSPEC-7` filter provided $1.84-2.63$ μm wavelength range, with native spectral resolution of $R \equiv \frac{\lambda}{\delta\lambda} = 1250$ from a $0\farcs76$ (4 pixels) $\times$ $42\farcs0$ slit. The individual epochs were coadded to form a single composite spectrum of signal to noise ratio $S/N \sim 30$ per pixel.

The reduced spectrum contained H_2 lines indicative of excited gas emission.These lines were fitted and removed from the spectrum to produce a composite sprectrum assumed to possess only stellar photosphere and circumstellar disk emission.

todo: T.P.G data reduction text:

1. Night sky lines as possible correlated residual structure
2. etc.

3. METHOD

Our analysis approach involves Bayesian forward modeling of the observed spectrum under a range of different assumptions about the protostellar system. We discuss the limitations of our assumptions in the discussion section.

3.1. *Composite spectrum forward model*

We assume that stellar photosphere and warm circumstellar disk emission dominate the radiation in the near-IR $K-$band. We constructed a forward model for the observed Keck spectrum using the spectral inference framework `Starfish` from Czekala et al. (2015, hereafter `C15`) with support for mixture model modifications similar to Gully-Santiago et al. (2017). The mixture model for S68N's Keck spectrum is:

$$S_{\lambda,\mathrm{mix}} = \Omega_\star I_\lambda(\boldsymbol{\theta}_*) + \Omega_\mathrm{d} B_\lambda(T_\mathrm{d}) \tag{1}$$

where $\boldsymbol{\theta}_* = (T_\mathrm{eff}, \log g, [\mathrm{Fe/H}])$ are the protostellar photospheric parameters, and I_λ and B_λ are spectral irradiances for the star and disk respectively. Assuming the star and disk emission originate at the same distance d, the ratio of solid angles relates the projected area of the emission regions.

$$\frac{\Omega_d}{\Omega_\star} = \frac{A_d d^2}{A_\star d^2} = \frac{A_d}{A_\star} \tag{2}$$

We model the protostellar spectral radiance $I_\lambda(T_\star)$ with Phoenix synthetic model spectra (Husser et al. 2013) possessing an unknown-but-low surface gravity $\log g \in [2.0, 4.0]$ in cm/s^2 and an effective temperature $T_\mathrm{eff} \in [2700, 3600]$ K. We assume metallicity is negligibly close to solar. The circumstellar disk irradiance is assumed to be black body, with a temperature range $T_\mathrm{d} \in [1000, 1500]$ K capped by the temperature at which typical dust sublimates.

The radiated spectrum passes through an unknown amount of extinction and scattering, altering its spectral shape in an uncertain—and potentially irretrievable—way. Nevertheless, we characterize the reddening with an A_K and a power law slope:

$$A_\lambda / A_K = \frac{\lambda}{2.2\ \mu\mathrm{m}}^{-\alpha}$$

with $\alpha \in [1.7, 2]$ representing the power law exponent that may depend on dust properties and degree of extinction (Moore et al. 2005).

The wavelength-domain follows a similar scaling to Czekala et al. (2015), with slight modification. Here we remove the $v \sin i$ broadening kernel, since the $R \sim 1250$ spectral resolution is too low to provide a meaningful constraint on projected stellar rotation. Instead, we replace $v \sin i$ with a nuisance parameter to characterize the uncertainty in effective instrumental spectral resolution broadening kernel $\mathcal{F}_v^\mathrm{inst}$, parameterized as small perturbations from our estimated instrumental resolution $\delta v_\mathrm{eff}^2 = (240\ \mathrm{km\ s^{-1}})^2 \pm \epsilon^2$. The instrumental-broadened mixture model is then:

$$S(\boldsymbol{\theta}_*, \delta v, v_r) = S_{\lambda,\mathrm{mix}} * \mathcal{F}_v^\mathrm{inst} * \mathcal{F}_v^\mathrm{dop} \tag{3}$$

The Doppler shift is similarly treated as a nuisance parameter, but is nonetheless included in the model to provide robustness in the face of imperfect instrumental calibration. We also apply a third order Chebyshev

polynomial with parameters c^i, and the same flexible covariance matrix C as in `C15`. Extinction and re-sampling proceed identically to `C15` to produce a pixel-level forward model M, containing 16 parameters.

We assume there is zero emission attributable to mass accretion onto the star or disk. This assumption almost certainly fails for Class 0 protostars, which are still actively accreting a large fraction of their mass. See §5 for discussion of the limitations of the model assumptions.

3.2. *MCMC details*

We used MCMC ensemble sampling to deliver a joint posterior probability distribution function for the astrophysical, instrumental, and nuissance parameters. The method employs `emcee` (Foreman-Mackey et al. 2013) to provide resilience against sampling strongly degenerate parameters such as solid angles and temperatures of the mixture model. We ran the MCMC sampler with 5000 steps and 40 walkers, selecting the final $\sim 200-1000$ steps as adequately devoid of hysteresis from initial conditions.

4. RESULTS

4.1. *Reasonable Effective Temperature*

The Baraffe et al. (2015) model tracks do not extend to ages < 1 Myr, but we expect the range of effective temperatures at such young ages to be comparable to the projections at 1 Myr based on extensions to the Hayashi track. If so, the range of temperatures derived for S68N place it in the expected range of protostars. Notably, we only searched for effective temperatures in the range $T_{\rm eff} \in [2700, 3600]$ K, so our method was unable to probe higher or lower possible temperatures. However our posterior samples do not "pile-up" near the parameter ranges as one would observe in an overly-restrictive parameter range. Instead our smooth posterior places most of its support in the middle of the effective temperature range.

4.2. *Low inferred surface gravity and comparison to evolutionary models*

We find a surface gravity in the range of $\log g = 2.x - 3.x$, marginalizing over all other (uncertain) stellar, disk, and nuissance parameters. This low alebit uncertain surface gravity places the object in the realm of low mass protostars– still undergoing gravitational contraction and accretion, and therefore possessing a relatively large radius with only a faction of its fated stellar mass. Figure 1 shows a two panel plot of the joint posterior on stellar surface gravity and effective temperature. Theoretical pre-main sequence stellar evolutionary model tracks computed for ages > 1 Myr (Baraffe et al. 2015) occupy regions with $2800 < T_{\rm eff}({\rm K}) < 4000$ and $3.3 < \log g$. Surface gravities lower than this 3.3 threshold should presumably be less evolved and younger protostars. Observations roughly agree. For example, the ~ 2 Myr IC348 occupies a space around $3.3 < \log g < 4.2$, while the $\sim 120 Myr$ Pleiades resides around $\log g \sim 4.5$, with warmer average temperatures. Class I protostars (Doppmann et al. 2005) occupy a broad range of measured and constrained effective temperatures and surface gravities, with relatively large uncertainties owing to the difficulty of simultaneously assigning surface gravity in the face of uncertain veiling measurements.

The joint, marginalized, posterior probability distribution for S68N is shown in the right panel of Figure 1.

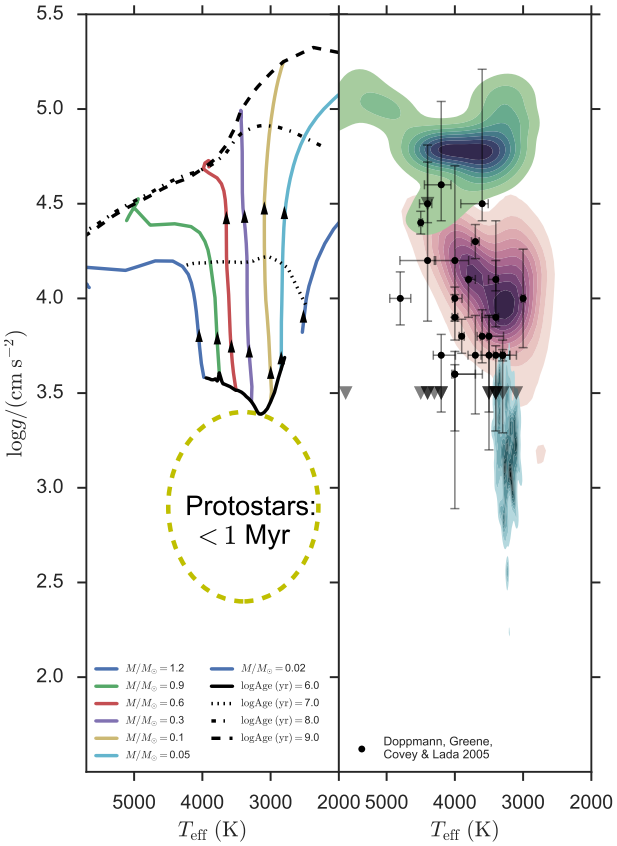

FIG. 1.— Pre-main sequence and protostar evolution comparison between theory (left panel) and obseration (right panel). The $0.02-1.2$ $M_\odot$ evolutionary model tracks are from Baraffe et al. (2015), spanning 1 Myr to 1 Gyr isochrones; protostars are expected to sit below the 1 Myr isochrone in the region of parameter space demarcated with a yellow dashed ellipse. The observations show coarse agreement with the models– measurements of the Pleiades from Cottaar et al. (2014, green KDE) cluster around the 100 Myr isochrone, although extend into higher-than-predicted $\log g$ for hotter stars. The younger IC348 sources (Cottaar et al. 2014, purple KDE) cluster with a large spread above and below the ~ 10 Myr isochrone. The source S 68N has a broad posterior PDF placing its maximum a-posteriori estimate inside the range of protostars. The black dots are Class I protostars from Doppmann et al. (2005), showing a large range in measured properties with relatively large uncertainties in $\log g$.

The majority of probability density is below all previous measurements.

4.3. *Constraints on disk/envelope emission*

The observed S68N spectrum is consistent with modest veiling from an extra smooth emission component, presumably either a circumstellar disk or envelope reradiating reprocessed starlight. The traditional observational metric for assessing veiling is the so-called r_λ-factor, the ratio of disk to photospheric flux, with the photospheric flux usually defined as the continuum. The right thing to do would be to compute the veiling by integrating the ratios of our forward modeled disk and photosphere spectrum over a relevant filter curve:

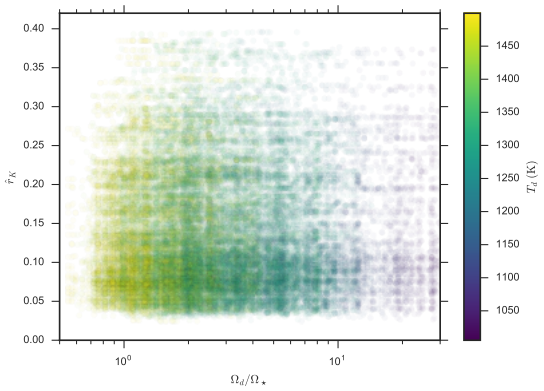

FIG. 2.— The projected joint distribution of $\hat{r}_K$ with disk to star solid angle ratio and characteristic disk temperature.

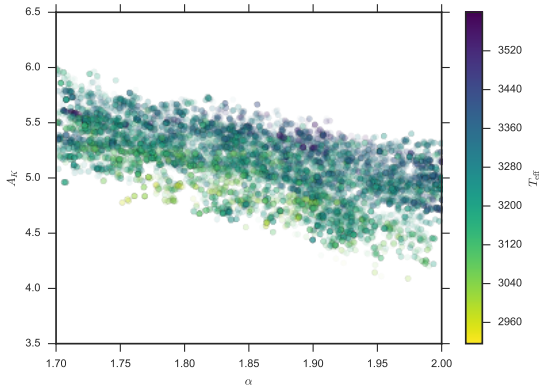

FIG. 3.— Extinction and power law slope distributions, with effective temperature dependence.

$$r_K = \int_K \frac{f_d}{f_\star} t(\lambda) d\lambda \tag{4}$$

where $t(\lambda)$ is the normalized wavelength-dependent transmission of the filter. In practice our observation band does not extend to the ends of $K-$band, so the accuracy of such an estimate would be limited to our projected flux ratio outside the observation window. So instead, we simply report the median pixel of the r_λ vector in our band $\hat{r}_K = r_\lambda|_{50\%}$, which coarsely approximates r_K. In practice, the distribution of $\hat{r}_K$ is much larger than the uncertainty attributable to this approximation. We find a distribution of $\hat{r}_K \in [0, 0.4]$, with a peak near 0.

The simplistic black body model allows the construction of the relative emitting areas of disk to star as defined in Equation 2. The relative areas are strongly dependent upon the assumptions of the effective temperatures of the star and disk. Figure 2 demonstrates one projection of the degenerate hyperspace relating disk temperature, solid angle ratio, and $\hat{r}_K$. Disk temperatures of $T_d \sim 1500$ (K) result in emitting areas of the disk comparable to the projected area of the stellar photosphere, and providing much less disk flux than photosphere flux.

4.4. *High extinction*

The Keck NIRSPEC spectrum of S68N shows a spectral flux density increasing with wavelength. The Phoenix photopheric model predicts a spectral flux density decreasing with wavelength for the range of best fit photospheric temperatures. The red slope indicates a high degree of reddening. Our posterior constraints confirm large values of extinction indicative of either a highly embedded source or a background object. Figure 3 shows the joint constraint on A_K and α, the power law extinction slope.

4.5. *SMM1*

We also performed spectral inference on the source SMM1, a less embedded protostar showing less-conspicuous CO lines in its NIRSPEC $K-$band spectrum. The conditions of the inference we identical to those of S68N, namely the same stellar and nuissance parameter ranges and priors. We ran the MCMC sampling for a total of 20000 steps, discarding the first 15000 as burn-in. Figure 6 shows the spectrum of SMM1 with a model

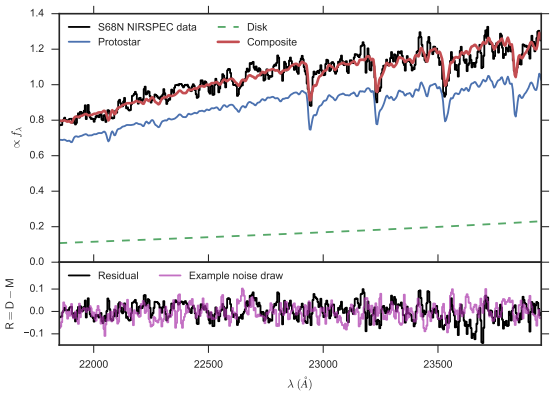

FIG. 4.— Observed and modeled spectrum of S68N with residual noise spectrum.

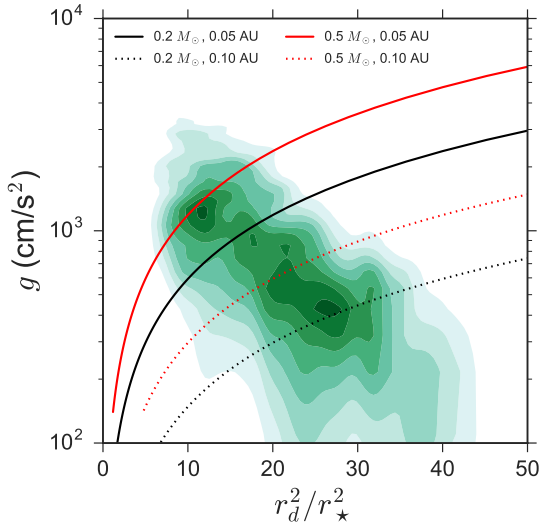

FIG. 5.— Posterior probability distribution function from Experiment 3, Run1, marginalized over all stellar and nuisance parameters except $\log g$ and $\Omega_d/\Omega_\star$. The surface gravity correlates with the solid angle ratio since both of these factors affect the CO line depths. Lines of differing stellar mass and disk radii are shown for a range of stellar radii.

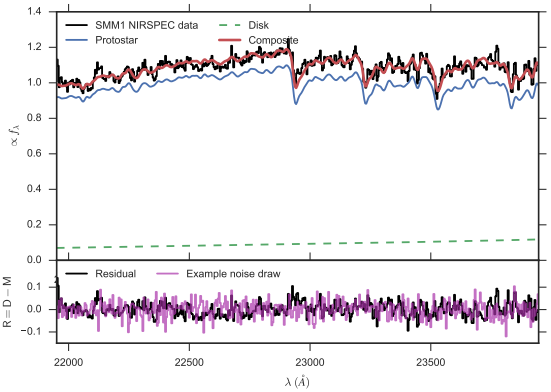

FIG. 6.— Observed and modeled spectrum of SMM1 with residual noise spectrum.

spectrum possessing parameters randomly chosen from its posterior samples.

		Marginal PDF		
Parameter	Description	$\lfloor_{16\%}$	Median	$\lfloor_{84\%}$
$T_{\rm eff}$	Stellar effective temperature (K)	3000	3200	3600
$\log g$	Surface gravity	2	3	4
v_r	Velocity error	-	-	-
ϵ	Resolution error	-	-	-
$\Omega_\star/\Omega_d$	Star/Disk solid angle ratio	-	-	-
$\hat{r}_K$	Estimated $K-$band veiling	-	-	-
T_d	Black body disk temperature	-	-	-
A_K	$K-$band extinction	-	-	-
α	Exponent of reddening law	-	-	-
$a_{\rm G}$	GP covariance kernel amplitude	-	-	-
ℓ	GP covariance kernel scale length	-	-	-

5. DISCUSSION

Our spectral inference methodology made some necessary simplifying assumptions in order to assess the relative strengths of the components giving rise to the observed, composite Keck NIRSPEC spectrum of S68N. Below we list the assumptions in order of how *strong* they are, and gauge their impact on our results.

1. There is no other emission source, other than photosphere and black body disk. Particularly, line emission veiling and accretion continuum veiling are ignored.
2. Phoenix models approximate emission of protostellar photospheres.
3. The photospheric temperature is in the range $T_{\rm eff} \in [2700, 3600]$ K.
4. The disk radiates as a single component black body in the range $T_{\rm d} \in [1000, 1500]$ K.
5. The disk and stellar photosphere undergo the same extinction wavelength dependence and extent.
6. A single correlation scale length and amplitude characterizes the noise model mismatch between model and data.
7. Metallicity departs negligibly from Solar.

We know other emission sources, beyond quiescent photosphere and disk. The raw spectrum of S68N shows H_2 emission lines indicative of either shocked material or accretion. Higher spectral resolution observations of protostars have shown CO emission (Lee et al. 2016). With our NIRSPEC observations alone, it is impossible to assess whether CO emission partially fills in the CO lines at $2.3 - 2.4$ μm. Such line veiling would tend to reduce the equivalent widths of the CO lines, and bias our presumed accretion-free estimate towards either *higher* surface gravity or *higher* veiling. In other words, the "true" surface gravity and veiling is lower than our posterior would suggest. We already derive a very low surface gravity, so it would be hard to imagine an even lower number, reinforcing our assumption in the first place.

Our model employs spectrally emulated Phoenix models to simulate the photospheric emission of S68N. Template photospheres of Class 0 protostars are not yet available due to the prohibitive difficulty of observations with existing facilities and high veiling. Protostellar photospheric emission could depart from Phoenix models based on non-standard physics not currently included in the stellar atmospheric modelling. For example strong magnetic fields, starspots, and other factors would alter the photospheric emergent spectrum's appearance from what we have assumed here. These non-standard physical phenomena would largely impact relatively weak features of the spectral mostly perceptible at higher spectral resolution. A large coverage fraction of cool starspots could distort our derived protostellar solid angle towards lower values and higher effective temperatures than reality. The physical effects of starspots on more evolved Class II and Class III stars are still actively being studied `cite gully-santiago, fang, etc.`, so it is not clear how Class 0 protostars compare.

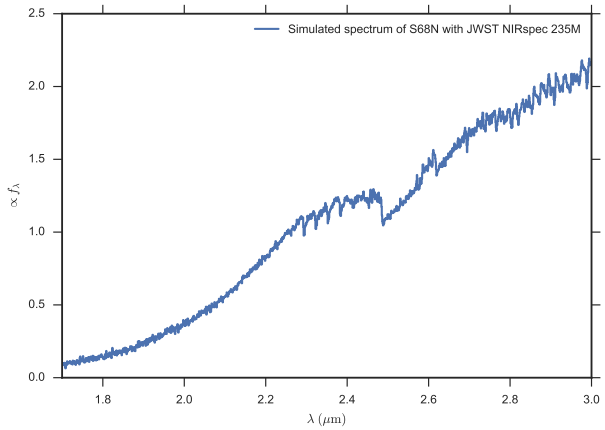

FIG. 7.— Simulated JWST observation of S68N.

We have assumed the disk radiates as a black body of a single temperature. More accurate estimates for the disk emission and geometries could be obtained from rigorous radiative transfer methods (Robitaille 2017, *e.g.*); no such advanced disk modeling was attempted. The relatively narrow $K-$ observation band does not offer a large enough lever arm to distinguish the nearly degenerate effects of elevated disk temperature versus increased solid angle of emission. It is unlikely that our limited spectral-grasp data would be able to place informative constraints on even more disk properties, nor would those revised models improve our fit quality significantly. Although the black body model was a simplifying assumption, it has produced a reasonable solid angle ratio posterior distribution.

We have assumed the disk and protostar undergo the same extent and wavelength-dependence of extinction. In principle, the starlight pass through a flared circumestellar disk or envelope, while the disk emission passess through relatively less (or more) material, causing differential extinction between disk and star. The relatively small solid angle ratio of the disk suggests that if the disk emitting material is distributed in an azimuthally symmetric ring around the star, the disk should be quite close to the protostellar surface, reinforcing our assumption that the emission sources pass through the same material.

5.1. *Simulated JWST Observations of S68N*

Below is a simulated spectrum of S68N with the JWST NIRSpec IFU with the G235M grating providing $R \sim 1000$ across $1.7 - 3.0$ μm, with a $S/N \sim 100$ per pixel.

TABLE 1
Experiment log

Exp. #	Run. #	Desc.	Outcome
1	1	Original, flawed `star_veil.py` code modeled disk radiance as a constant value with no physical interpretation	Exposed need for more physical inputs
2	1	Run with `star_BB.py` code with erroneous Ω prescription, weak priors, poor first guess	Exposed need for better priors and starting guess
2	2	Run with `star_BB.py` code with erroneous Ω prescription, strong priors (T_d fixed to ~ 1100 K), good first guess	Exposed incorrect Ω treatment
3	1	Run with `star_BB.py` code with correct absolute flux level, strong priors (T_d fixed to ~ 1100 K).	Reasonable results, weak constraints on $\log g$.
3	2	Run with `star_BB.py` code with correct absolute flux level, *weak* priors (T_d variable $\in [1000, 1700]$ K).	–
4	1	Reduced spectral range to enhance $\log g$ sensitivity	Good convergence, wide posteriors
5	1	Windowing on CO and Na I, T_d fixed to ~ 1100 K	Slightly higher $T_{\rm eff}$ and $\log g$ compared to just CO window.
6	1	Introduce A_V, with fixed ($\alpha = -2.0$) slope, $\log g > 2.0$, Chebyshev 6% peak-to-valley	Tighter T_{eff} and $\log g$ posteriors than before
7	1	A_V, with variable ($\alpha \in [-2.0, -1.7]$) slope, $\log g > 2.0$, Chebyshev 2% peak-to-valley	Tighter T_{eff} and $\log g$ posteriors due to tighter Chebyshev, α limit exceeded
8	1	A_K, with variable ($\alpha \in [-2.0, -1.7]$) slope, $\log g > 2.0$, Chebyshev 2% peak-to-valley	Re-running

APPENDIX

ADAPTATIONS OF STARFISH TO HANDLE ABSOLUTE FLUX AND SOLID ANGLE

The original `Starfish` framework flux-standardized its emulated spectra to remove uninteresting correlations in effective temperature and solid angle. Here we return the mean flux levels to provide an accurate estimate of Ω.

Experiments

We tried several experiments:

We thank the Keck telescope staff.
Facilities: Keck (NIRSPEC)
Software: *pandas* (McKinney 2010), *emcee* (Foreman-Mackey et al. 2013), *matplotlib* (Hunter 2007), *numpy* (Walt et al. 2011), *scipy* (Jones et al. 2001–), *ipython* (Pérez & Granger 2007), *starfish* (Czekala et al. 2015), *seaborn* (Waskom et al. 2014)

REFERENCES

Baraffe, I., Homeier, D., Allard, F., & Chabrier, G. 2015, A&A, 577, A42
Cottaar, M., Covey, K. R., Meyer, M. R., et al. 2014, ApJ, 794, 125
Czekala, I., Andrews, S. M., Mandel, K. S., Hogg, D. W., & Green, G. M. 2015, ApJ, 812, 128
Doppmann, G. W., Greene, T. P., Covey, K. R., & Lada, C. J. 2005, AJ, 130, 1145
Foreman-Mackey, D., Hogg, D. W., Lang, D., & Goodman, J. 2013, PASP, 125, 306
Gully-Santiago, M. A., Herczeg, G. J., Czekala, I., et al. 2017, ApJ, 836, 200
Hunter, J. D. 2007, Computing in Science and Engineering, 9, 90
Husser, T.-O., Wende-von Berg, S., Dreizler, S., et al. 2013, A&A, 553, A6
Jones, E., Oliphant, T., Peterson, P., et al. 2001–, SciPy: Open source scientific tools for Python, [Online; accessed 2016-08-02]
Lee, S., Lee, J.-E., Park, S., et al. 2016, ApJ, 826, 179
McKinney, W. 2010, in Proceedings of the 9th Python in Science Conference, ed. S. van der Walt & J. Millman, 51 – 56
Moore, T. J. T., Lumsden, S. L., Ridge, N. A., & Puxley, P. J. 2005, MNRAS, 359, 589
Pérez, F., & Granger, B. E. 2007, Computing in Science and Engineering, 9, 21
Robitaille, T. P. 2017, ArXiv e-prints, arXiv:1703.05765
Walt, S. v. d., Colbert, S. C., & Varoquaux, G. 2011, Computing in Science and Engineering, 13, 22
Waskom, M., Botvinnik, O., Hobson, P., et al. 2014, seaborn: v0.5.0 (November 2014), doi:10.5281/zenodo.12710